M. A. Dakka, G. Tsiminis, R. D. Glover, C. Perrella, J. Moffatt, N. A. Spooner, R. T. Sang, P. S. Light, and A. N. Luiten
Laser-based metastable krypton generation
Physical Review Letters, 2018; 121(9):093201-1-093201-6

Originally published by American Physical Society at:
http://dx.doi.org/10.1103/PhysRevLett.121.093201

Laser-based metastable krypton generation

M.A. Dakka[1], G. Tsiminis[1,2], R.D. Glover[3], C. Perrella[1], J. Moffatt[1,2],
N.A. Spooner[1,2,4], R.T. Sang[3], P.S. Light[1] and A.N. Luiten[1]
[1] *Institute for Photonics and Advanced Sensing, School of Physical Sciences, University of Adelaide, SA 5000 Australia*
[2] *Cooperative Research Centre for Optimising Resource Extraction, School of Physical Sciences, University of Adelaide, SA 5000 Australia*
[3] *Centre for Quantum Dynamics, School of Natural Sciences, Griffith University, QLD 4111, Australia*
[4] *Defence Science and Technology Group, PO Box 1500, SA 5111, Australia*
(Dated: May 16, 2018)

We demonstrate the generation of metastable krypton in the long-lived $1s^5$ state using laser excitation. The atoms are excited through a two-photon absorption process into the $2p^6$ state using a pulsed optical parametric oscillator laser operating near 215 nm, after which the atoms decay quickly into the metastable state with a branching ratio of 75 %. The interaction dynamics are modeled using density matrix formalism and, by combining this with experimental observations, we are able to calculate photo-ionization and two-photon absorption cross-sections. When compared to traditional approaches to metastable production, this new approach shows great potential for high-density metastable krypton production with minimal heating of the sample. The estimated metastable production efficiency in this experiment was 2 % per pulse with the model suggesting fractional efficiencies up to 30 % are possible under optimal conditions.

INTRODUCTION

Metastable noble gas atoms [1] have found wide use since the advent of laser manipulation of atoms, with diverse applications including atom lithography [2], rare isotope detection [3–6], Bose-Einstein condensation [7], optically pumped rare gas lasers [8], nonlinear optics [9–11], and the search for nuclear electric dipole moment [12, 13]. Metastable krypton (Kr^*), in particular, is important for sum-frequency generation of tunable vacuum-UV radiation [9–11] and for radiokrypton dating [14–16].

These applications all require an experimental step to prepare the target into the relevant high energy (10-20 eV) metastable state. Primarily, direct-current (DC) and radio-frequency (RF) discharge sources are used [17–19], which are limited by poor (10^{-4}) average efficiency [20] and require a minimum gas density to operate. This minimum gas density requirement means that typically the discharge source is situated some distance from the experimental chamber and a series of specialized equipment is required to extract and transport the metastable atoms [21]. Previously all-optical approaches have been shown to circumvent this pressure requirement but have so far not demonstrated an increase in efficiency [22]. Furthermore, for certain applications, the sputtering of highly charged, electro-statically accelerated noble gas ions (11-25 eV) onto the surface of the vacuum chamber can lead to slow outgassing and unwanted cross-contamination between samples [14]. Other production methods such as electron beam bombardment [23, 24], charge transfer [21, 25], and two-step optical pumping [22, 26–29] are limited by space charge limitations, short source lifetimes due to sputtering, and reliance on an initial discharge or electron-impact sources (inheriting some of the disadvantages of these sources), respectively [21].

The work here describes a direct optical excitation approach only possible using deep-UV (DUV) laser technology. This work is expected to avoid the major deficiencies of the discharge approaches - in particular, leading to higher efficiencies and also preventing sample cross-contamination. Here we target a two-photon transition in krypton to access a high-lying excited state, which decays quickly (25 ns lifetime) into the desired metastable state with a high branching ratio ($\beta \approx 75\,\%$), although the level structures of all the noble gas species are equally suitable, provided a laser is available at the required wavelength. This Letter reports on a comprehensive investigation of pulsed Kr^* production using a 215 nm laser by varying both the power and detuning of the laser excitation. We support observations with density matrix (DM) calculations that allow us to calculate the two-photon and photo-ionization cross-sections.

APPARATUS AND PROCEDURE

The approach of this work is shown on Fig. 1, where 215 nm light excites a two-photon transition into a short-lived $2p^6$ state. The 215 nm radiation is generated by frequency doubling a commercial optical parametric oscillator (OPO) that can be tuned from 410 nm-2500 nm. The output of the frequency-doubled OPO is a 5 ns DUV pulse with a maximum pulse energy E_p of 2 mJ over a 200 GHz bandwidth. The laser pulses are focused by a 75 mm CaF_2 lens to a 100 µm spot at the center of a quartz gas cell filled with krypton gas at a pressure of 0.05 mbar. The gas cell is sealed with uncoated 2° wedge windows made of UV grade SiO_2 that have been attached at an 11° angle to minimize back-reflection. The UV pulse energy was directly monitored by intercepting the beam with a UV power meter, while the wavelength was

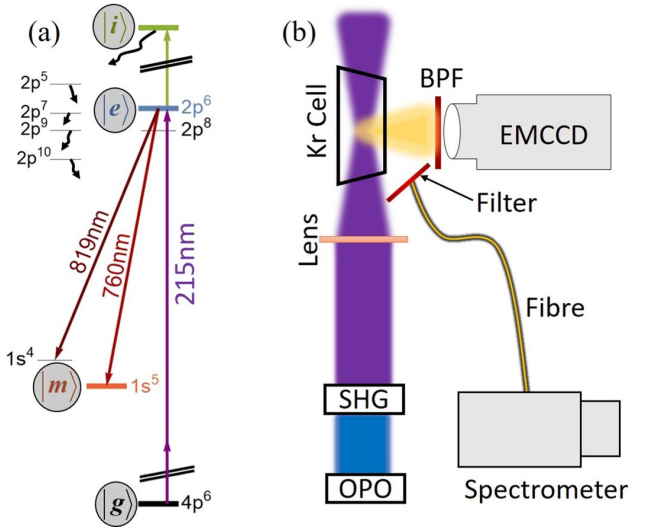

FIG. 1: (a) Partial energy level diagram of krypton. Levels in the theory section of this paper are circled: ground $|g\rangle$, excited $|e\rangle$, metastable $|m\rangle$, ionized $|i\rangle$. (b) Laser-induced fluorescence (LIF) detection apparatus.

ascertained by measuring the direct output of the OPO (at ∼429 nm) with a spectrometer.

Images of the laser-induced fluorescence (LIF) at 760 nm and 819 nm (from decay into the $1s^5$ and $1s^4$ states, respectively) are collected by an EMCCD camera positioned 95 mm from the laser beam focal region. To select between the two signals and reject scattered pump light and fluorescence from other decay routes we have fitted 760 nm and 820 nm bandpass filters (10 nm FWHM) to the front surface of an apochromatic camera lens. Assuming isotropic fluorescence, the total effective collection efficiency, including solid angle and losses in the optical collection system, is 0.1 %. The SNR of each image was improved by averaging 5 frames that were each of 5 s exposure time (a total of 250 pulses). In addition to the EMCCD measurements, a spectrometer collected the LIF via a multimode optical fiber.

Under the following conditions, the 760 nm LIF can be closely related to the total metastable population produced by a laser pulse: the laser intensities used are well below the limit at which the laser field begins to exceed the binding energy of a valence Kr electron, the photo-ionization rate from the metastable state is negligible [30], and relatively low pressure (0.05 mbar) means that collisional losses are negligible [17]. This gives us the means to produce a simple relation between the 760 nm LIF and the two-photon absorption cross-section, $\sigma_0^{(2)}$.

RESULTS

We measured the spectral content of the LIF and noted multiple fluorescent peaks (Fig. 2). The branching ratio β out of the $2p^6$ excited state is calculated by taking the ratio of integrated intensities in the 760 nm and 819 nm LIF peaks, giving $\beta = (75 \pm 4)\,\%$. The uncertainty arises from uncertainty in the wavelength-dependent quantum efficiency of the spectrometer CCD. This value is consistent with reported values for this transition [26, 27, 31–39], but with improved uncertainty (see Table I).

Additional peaks noted in the LIF spectrum arise from resonance-enhanced multi-photon ionization (REMPI) followed by dissociative recombination through the 5p-5s transition band [40]. These peaks are seen to disappear with lower excitation energy as shown in Fig. 2. The strongest such peaks come from decay channels via $2p^9$-$1s^5$ (811.5 nm), $2p^2$-$1s^2$ (826.5 nm), and $2p^7$-$1s^4$ (830.0 nm) transitions, labeled a-c in Fig. 2.

Figure 3 shows EMCCD images of the fluorescence intensity emitted from the side of the gas cell under a range of different input pulse energies. We see a range of interesting nonlinear behaviours at higher energies. The top image from panel (a) in Fig. 3 shows filamentation, or re-focusing, which occurs for laser intensities that rapidly (∼1 ns) photo-ionize a significant fraction of the atoms within the laser beam [41]. We also note the halo shape surrounding the beam waist region (2mJ images in Fig. 3(b) and more weakly in the 1mJ images) that is likely due to space charge effects created by the intense pulse [42–44], and the subsequent (∼ 5 µs) fluorescence from dissociative recombination [41].

In order to compare the experimental results to the theoretical model we translate the absolute photon counts from EMCCD image into a total emitted photon number per pulse from a representative volume. This volume is centered on the waist and has boundaries set by the location with input intensity within 10 % of the maximum (see Fig. 3(a)). The emitted LIF photon number is then divided by the number of atoms (40×10^7 atoms) inside the interaction volume (6.0×10^{-6} cm^3) to yield

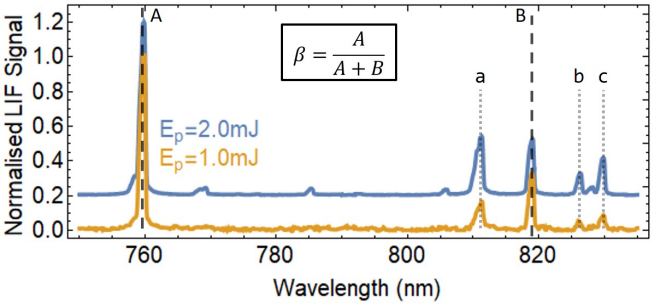

FIG. 2: LIF spectra for pump energies of (a) 2 mJ (vertically offset for clarity) and (b) 1 mJ, showing evidence of dissociative recombination peaks. The strongest measured recombination transitions are a) $2p^9$-$1s^5$, b) $2p^2$-$1s^2$, and c) $2p^7$-$1s^4$. Branching ratio remains unchanged with varying laser energy.

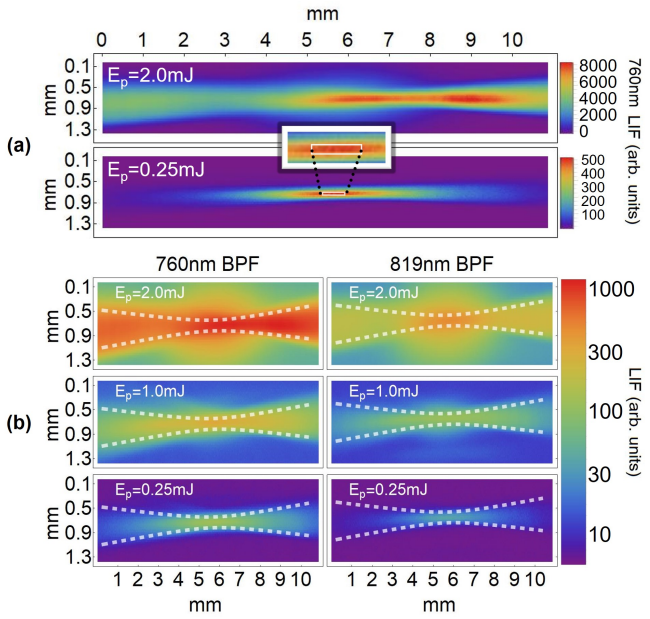

FIG. 3: (a) LIF images at 760 nm (scaled linearly to highlight spatial features) showing evidence of filamentation at higher energies. (b) Representative log scale images at 760 nm (left) and 819 nm (right) at 2.0mJ, 1.0mJ and 0.25mJ with e^{-2} beam diameter lines overlaid (white dotted). Beam direction is left to right.

an estimate of the LIF per atom, ρ_{LIF}. We estimate to have achieved a maximum ρ_{LIF} of 2 %.

THEORY AND ANALYSIS

The time-dependent model of a 4-level system, using the state designations shown in Fig. 1(a), is used to calculate the metastable population $\rho_{mm}(t)$. The dynamics are described by the governing Liouville equation [45]:

$$\dot{\rho}_{ab} = -\frac{i}{\hbar}[\hat{H}, \rho_{ab}] + \hat{\mathcal{L}}(\gamma_k, \rho_{ab}), \tag{1}$$

where $\hat{H}$ is the total interaction Hamiltonian and $\hat{\mathcal{L}}$ is the relaxation operator where the γ_k term represents relaxation rates. For $a = b$, $\rho_{aa} = |\langle a|a\rangle|^2$ is the probability of finding an atom in a given state $|a\rangle$, while for $a \neq b$, ρ_{ab} is the coherence term between states $|a\rangle$ and $|b\rangle$. In the scheme shown in Fig. 1(a), only the ρ_{eg} (and its conjugate) terms are non-vanishing, and since there are no intermediate states, the two-photon Rabi frequency $\Omega^{(2)}(t)$ can be related to the two-photon cross-section $\sigma_0^{(2)}$ and the laser intensity $I(t)$ by [46, 47]:

$$\Omega^{(2)}(t) = \sqrt{\frac{2}{\pi}\sigma_0^{(2)}}\frac{I(t)}{\hbar\omega_0}, \tag{2}$$

where $\hbar$ is the reduced Planck constant and ω_0 is the laser frequency. The model takes account of laser detuning Δ, laser decoherence [48–50], collisional effects [17] including Penning ionization [51, 52], spontaneous decay from the excited state [27], branching ratio, and photo-ionization. The photo-ionization rate from state $|j\rangle$ is related to the cross-section σ_{ji} as:

$$R_{ji} = \sigma_{ji}\frac{I(t)}{2\hbar\omega_0}, \tag{3}$$

where we note that the photo-ionization cross-section from the $1s^5$ state σ_{mi} is less than 3 % of that from the $2p^6$ state σ_{mi} [30]. We have thus neglected the former in the calculation as it does not significantly modify the metastable population.

For the relatively broad spectrum of the source used in this experiment, phase fluctuations (decoherence) play an important role in the excitation dynamics. We use the phase diffusion model [48–50] to average over these fluctuations, yielding a decoherence rate, γ_L:

$$\gamma_L = 2\sigma\frac{(b\sigma)^2}{(b\sigma)^2 + \Delta^2}, \tag{4}$$

where σ is the FWHM laser linewidth and b is a lineshape parameter (0.5 for an ideal Lorentzian lineshape and ~3 for the Gaussian lineshape of the 200 GHz linewidth laser used in this experiment [49]).

Figure 4 shows a sample of the time-evolution of population states under resonant excitation by a 0.25 mJ, laser pulse with a beam diameter of 100 µm, and a gas pressure of 0.05 mbar. Under these conditions, Kr* atoms are long-lived and thus we associate every detected 760 nm LIF photon with the production of a single Kr* atom. In this case, ρ_{LIF} is a direct measure of the steady-state fractional Kr* population $\rho_{mm}(t_{ss})$, where time $t = t_{ss}$

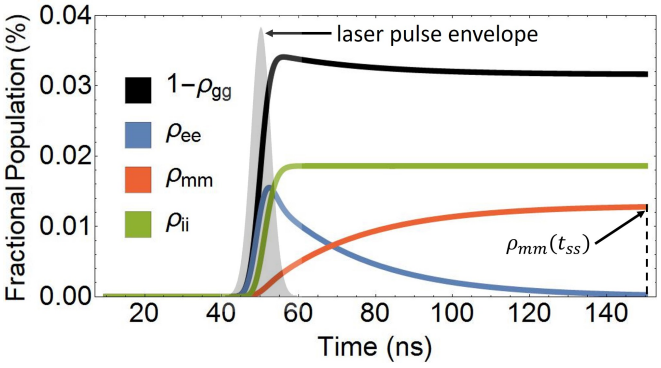

FIG. 4: DM population dynamics for ground ρ_{gg}, excited ρ_{ee}, metastable ρ_{mm}, and ionized ρ_{ii} states at 0.05 mbar, excited by a 5 ns pulse centered at 50 ns (pulse envelope highlighted in gray) with $E_p = 0.25$ mJ.

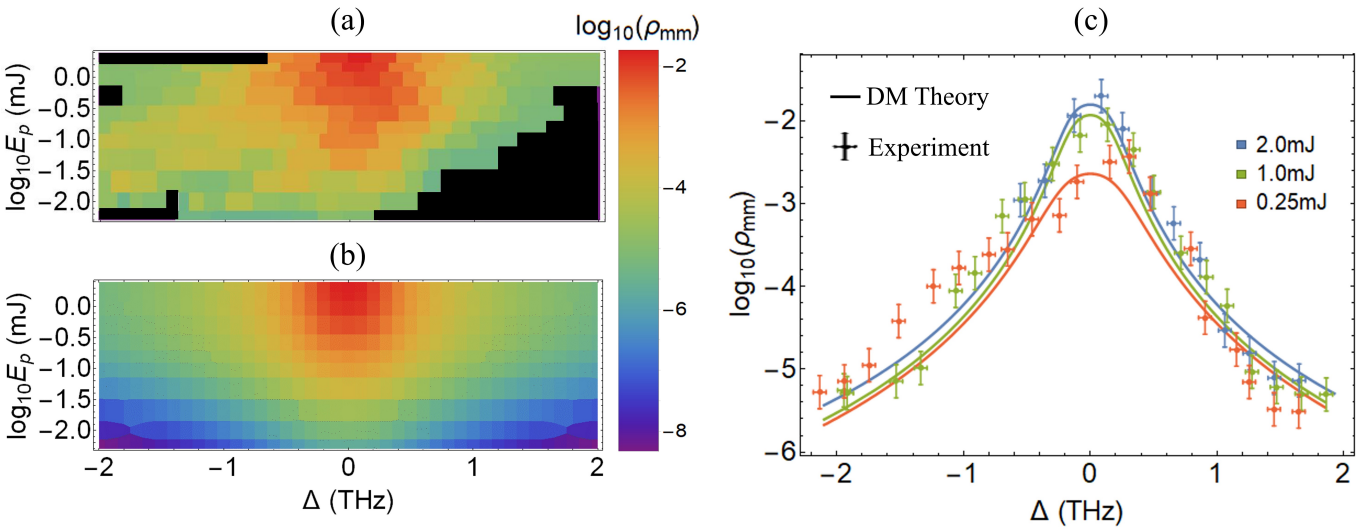

FIG. 5: (a) ρ_{LIF} (calculated from 760 nm LIF data) and (b) $\rho_{mm}(t_{ss})$ (fitted with theory) versus laser detuning, Δ, and energy, E_p. (c) Representative plots of experiment (points) vs. theory (lines) at 2mJ, 1.0mJ and 0.25mJ.

is long after pulse termination, and $\rho_{ee}(t_{ss}) \approx 0$. We note that the peak laser intensity used in this experiment ($1\,\mathrm{GW\,cm^{-2}}$) is well below the limit at which the laser field begins to exceed the binding energy of a valence Kr electron (a few $\mathrm{PW\,cm^{-2}}$) and under the threshold for significant population redistribution to occur [53].

We use the experimental data to derive the two-photon absorption cross-section, $\sigma_0^{(2)}$, and photo-ionization cross-section from the $2p^6$ state σ_{ei} (see Table I) by a non-linear fitting to the predictions of the density matrix model. The fitting approach is based on the minimum root mean squared error method by varying $\sigma_0^{(2)}$ and σ_{ei}. A comparison between experimental and theoretical results based on this approach is shown in Fig. 5.

We note the presence of some subtle lineshape asymmetry as well as features on the low frequency wing in the experimental data of Fig. 5(c). These are repeatable and more pronounced when using medium and lower energy excitation. The origin of these effects is not definite although potentially these arise from imperfections in the excitation laser source.

To the authors' knowledge, this is the only experimental measurement of the $\sigma_0^{(2)}$ for krypton, although we note from Table I that it is similar to the analogous transition in xenon [41]. The derived photo-ionization cross-section also agrees well with a previous theoretical estimate of this value [30].

Figure 6 shows extrapolation of theoretical Kr^* production rates for three laser linewidths and varying pulse energies. In the low energy ($< 200\,\mu J$) and mid-to-large linewidth regime (10 GHz and 200 GHz), phase fluctuations dominate and $\rho_{mm} \propto E_p^2$. For the Fourier transform limited linewidth (~250 MHz) only 100 µJ is required to achieve 30 % per efficiency pulse. In all cases, photo-ionization from the $2p^6$ state begins to dominate at high laser intensities, decreasing Kr^* population. This shows that simply increasing the intensity does not necessarily lead to improved efficiency of Kr^* production. The interplay between excitation, photo-ionization and decay rates must be balanced to optimize Kr^* production.

TABLE I: Comparing experiment to literature for branching ratio and cross-section values.

Reference	β (%)	$\sigma_0^{(2)}$, ($10^{-35}\mathrm{cm}^4$)	σ_{ei}, ($10^{-18}\mathrm{cm}^2$)
This work	75 ± 4	5.2 ± 2.1	3.8 ± 1.7
Literature	76 ± 3[a]	2.4 ± 0.8[b]	3.3[c]

[a] Estimate written here is the average deviation of the values, although quoted uncertainties are much larger [26, 27, 31–39].
[b] The ground-$2p^6$ transition of Xe. [41]. Not directly comparable.
[c] Calculated from [30].

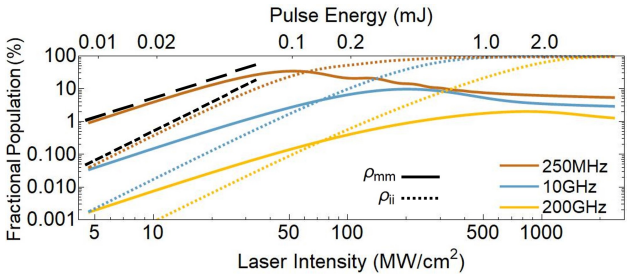

FIG. 6: Theoretical Kr^* (solid) and Kr^+ (dashed) fractional populations vs. laser intensity for several laser linewidths. In all cases the pulse duration is held at 5 ns. Intensity squared (long-dashed) and intensity cubed (short-dashed) lines are shown for reference.

DISCUSSION

The maximum metastable efficiency for the laser used in this experiment is around 10^{-2} per pulse, but one should consider the duty cycle of pulsed excitation to calculate the effective average density of metastable atoms. At a pressure of 0.05 mbar, the collisional lifetime of Kr^* atoms is a few μs, while the time between pulses in this experiment is $\sim$100 ms. However, improvements such as reducing laser linewidth (<10 GHz) and increasing repetition rate (>10 kHz) using pulse energies no greater than 20 µJ would enable quasi-CW operation with effective average density of metastable atoms above 10^{-4}.

With the use of DUV lasers, it is possible to ionize a significant fraction of irradiated excited atoms by absorption of an additional photon, especially in the presence of resonance conditions and high laser intensity ($>10\,\mathrm{GW\,cm^{-2}}$). The resultant population redistribution of the medium can modify the response of the system, destroying resonance conditions [53]. While such redistribution effects can introduce considerable uncertainty in the interpretation and analysis of experimental results at high intensities, the maximum laser intensity used in this experiment is an order of magnitude below this threshold. Although there is evidence of dissociative recombination at intensities as low as ($250\,\mathrm{MW\,cm^{-2}}$), the principal interaction effects are reasonably well captured by the phase diffusion model.

CONCLUSION

This paper demonstrates that two-photon laser excitation is a viable method to achieve Kr^* production efficiencies of $>10^{-2}$ per-pulse. We provide an experimental determination of the two-photon ground-$2p^6$ cross-section, which is similar to that of a similar transition in xenon. The photo-ionization cross-section, also determined experimentally, agrees well with previous literature. By improving the duty cycle and reducing gas pressure we expect that the rate of laser-based Kr^* production can be made competitive with state-of-the-art cw techniques.

[1] E. Muschlitz, Science **159**, 599 (1968).
[2] K. Berggren *et al.*, Science **269**, 1255 (1995).
[3] C. Chen, Science **286**, 1139 (1999).
[4] W. Jiang *et al.*, Phys. Rev. Lett. **106**, 103001 (2011).
[5] Z.-T. Lu *et al.*, Earth-Science Rev. **138**, 196 (2014).
[6] J. Zappala *et al.*, Water Resour. Res. **53**, 2553 (2017).
[7] A. Robert *et al.*, Science **292**, 461 (2001).
[8] W. Rawlins *et al.*, Opt. Exp. **23**, 4804 (2015).
[9] K. Bonin and T. McIlrath, J. Opt. Soc. Am. B **2**, 527 (1985).
[10] J. Marangos *et al.*, J. Opt. Soc. Am. B **7**, 1254 (1990).
[11] N. Saito *et al.*, Opt. Exp. **24**, 7566 (2016).
[12] M. Bishof *et al.*, Phys. Rev. C **94**, 025501 (2016).
[13] E. Altiere *et al.*, Phys. Rev. A **97**, 012507 (2018).
[14] W. Jiang *et al.*, Geochim. Cosmochim. Acta **91**, 1 (2012).
[15] L.-Y. Tu *et al.*, Anal. Chem. **86**, 4002 (2014).
[16] Z.-T. Lu, Nat. Sci. Rev. **3**, 172 (2016).
[17] H. Katori and F. Shimizu, Phys. Rev. Lett. **70** (1993).
[18] A. Palmer, M. Baker, and R. Sang, Rev. Sci. Instrum. **75**, 5056 (2004).
[19] C.-F. Cheng *et al.*, Rev. Sci. Instrum. **81**, 123106 (2010).
[20] X. Du *et al.*, Rev. Sci. Instrum. **75**, 3224 (2004).
[21] F. Dunning and R. Hulet, *Atomic, Molecular and Optical Physics: Atoms and Molecules* (Academic Press, NY, USA, 1996).
[22] M. Kohler *et al.*, EPL **108**, 13001 (2014).
[23] R. Freund, Rev. Sci. Instrum. **41**, 1213 (1970).
[24] M. Asgar Ali and P. Stone, Int. J. Mass Spect. **271**, 51 (2008).
[25] R. Neynaber and S. Tang, J. Chem. Phys. **70**, 4272 (1979).
[26] L. Young, D. Yang, and R. Dunford, J. Phys. B **35**, 8 (2002).
[27] Y. Ding *et al.*, Rev. Sci. Instrum. **78** (2007).
[28] H. Daerr *et al.*, Rev. Sci. Instrum. **82**, 073106 (2011).
[29] G. Hickman, J. Franson, and T. Pittman, Opt. Lett. **41**, 4372 (2016).
[30] H. Hyman, Appl. Phys. Lett. **31**, 14 (1977).
[31] P.-T. Anne and J. Chamberlain, Proc. Phys. Soc. **82**, 133 (1963).
[32] P. Murphy, J. Opt. Soc. Am. **58**, 1200 (1968).
[33] D. Landman and R. Dobrin, Phys. Rev. A **8**, 1868 (1973).
[34] J. Lemoigne, X. Husson, and J. Margerie, Opt. Commun. **15**, 241 (1975).
[35] R. Lilly, J. Opt. Soc. Am. **66**, 245 (1976).
[36] W. Ernst *et al.*, Physica **93C**, 136 (1978).
[37] M. Aymar and M. Coulombe, At. Data Nucl. Data Tables **21**, 537 (1978).
[38] R. Chang, H. Horiguchi, and D. Setser, J. Chem. Phys. **73**, 778 (1980).
[39] K. Dzierga *et al.*, Phys. Rev. A **62**, 022505 (2000).
[40] Y.-J. Shiu and M. Biondi, Phys. Rev. A **16**, 1817 (1977), pRA.
[41] S. Kroll and W. Bischel, Phys. Rev. A **41**, 1340 (1990).
[42] E. McDaniel and E. Mason, *The Mobility and Diffusion of Ions in Gases* (John Wiley & Sons, 1973).
[43] A. Tolmachev *et al.*, Anal. Chem. **81**, 4778 (2009).
[44] P. Neves, C. Conde, and L. Tavora, J. Chem. Phys. **133**, 124316 (2010).
[45] K. Blum, *Density Matrix Theory and its Applications* (Springer, New York, 2012).
[46] D. Bates and B. Bederson, *Advances in Atomic and Molecular Physics*, Vol. 12 (Elsevier, 1976).
[47] D. Bamford *et al.*, J. Opt. Soc. Am. B **5**, 1369 (1988).
[48] G. Agarwal, Phys. Rev. Lett. **37**, 1383 (1976).
[49] P. Zoller and P. Lambropoulos, J. Phys. B **12**, L547 (1979).
[50] B.-N. Dai and P. Lambropoulos, Phys. Rev. A **34**, 3954 (1986).
[51] R. Neynaber and G. Magnuson, Phys. Rev. A **14**, 961 (1976).
[52] K. Temelkov, N. Vuchkov, and N. Sabotinov, J. Phys.: Conference Series **44**, 116 (2006).
[53] M. Shahidi, T. Luk, and C. Rhodes, J. Opt. Soc. Am. B **5**, 2386 (1988).